JCTC Journal of Chemical Theory and Computation

pubs.acs.org/JCTC Article

Toward Quantum Chemical Free Energy Simulations of Platinum Nanoparticles on Titania Support

Van-Quan Vuong,* Ka Hung Lee, Aditya A. Savara, Victor Fung, and Stephan Irle*

Cite This: J. Chem. Theory Comput. 2023, 19, 6471−6483 Read Online

ACCESS | Metrics & More | Article Recommendations | Supporting Information

ABSTRACT: Platinum nanoparticles (Pt-NPs) supported on titania surfaces are costly but indispensable heterogeneous catalysts because of their highly effective and selective catalytic properties. Therefore, it is vital to understand their physicochemical processes during catalysis to optimize their use and to further develop better catalysts. However, simulating these dynamic processes is challenging due to the need for a reliable quantum chemical method to describe chemical bond breaking and bond formation during the processes but, at the same time, fast enough to sample a large number of configurations required to compute the corresponding free energy surfaces. Density functional theory (DFT) is often used to explore Pt-NPs; nonetheless, it is usually limited to some minimum-energy reaction pathways on static potential energy surfaces because of its high computational cost. We report here a combination of the density functional tight binding (DFTB) method as a fast but reliable approximation to DFT, the steered molecular dynamics (SMD) technique, and the Jarzynski equality to construct free energy surfaces of the temperature-dependent diffusion and growth of platinum particles on a titania surface. In particular, we present the parametrization for Pt-X (X = Pt, Ti, or O) interactions in the framework of the second-order DFTB method, using a previous parametrization for titania as a basis. The optimized parameter set was used to simulate the surface diffusion of a single platinum atom (Pt_1) and the growth of Pt_6 from Pt_5 and Pt_1 on the rutile (110) surface at three different temperatures (T = 400, 600, 800 K). The free energy profile was constructed by using over a hundred SMD trajectories for each process. We found that increasing the temperature has a minimal effect on the formation free energy; nevertheless, it significantly reduces the free energy barrier of Pt atom migration on the TiO_2 surface and the transition state (TS) of its deposition. In a concluding remark, the methodology opens the pathway to quantum chemical free energy simulations of Pt-NPs' temperature-dependent growth and other transformation processes on the titania support.

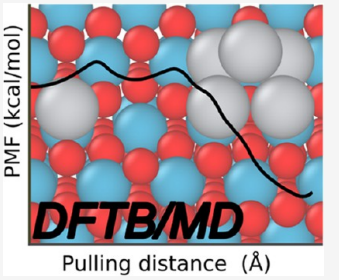

Downloaded via GEORGIA INST OF TECHNOLOGY on January 19, 2024 at 15:25:50 (UTC).
See https://pubs.acs.org/sharingguidelines for options on how to legitimately share published articles.

INTRODUCTION

The noble transition metal platinum (Pt) is well known for its highly effective and selective catalytic properties in heterogeneous and homogeneous catalysis. Pt-based heterogeneous catalysts are an indispensable part of automobile exhaust gas treatment, fertilizer manufacturing, hydrogen production, and fuel cells.[1−5] The effectiveness of heterogeneous catalysts is governed by their surface's atomic and electronic structures. Mid to late-transition metals do not typically wet oxide surfaces but typically form particles on oxide surfaces.[6,7] The size of heterogeneous catalyst particles has been found to be critical in controlling the catalytic performance of metals, affecting not only the catalyst particles' surface area but also the electronic structure, particularly for particles with diameters of up to 100 nm. With the advancement of nanoscience over the past decades, the use of size-tunable Pt nanoparticles (Pt-NPs), which have a specific surface area significantly higher than that of their bulk counterparts, has been greatly increased. Notably, Pt-NPs and Pt single atoms supported on titania surfaces have been used as effective heterogeneous catalysts in industrial processes.[8−11]

However, due to the elemental rarity on the planet, Pt is an expensive metal, making its application very costly. In addition, a significant challenge in using Pt nanoparticles and other precious metal nanoparticles is that the nanoparticles can undergo nucleation, sintering, Ostwald ripening, and adatom removal processes such that the catalyst must eventually be replaced.[12] Therefore, creating more durable Pt-based catalysts, particularly with reduced platinum, is one of the vital targets in heterogeneous catalysis.[13] For a rational design of new catalysts optimized for durability and catalytic properties, it is crucial to understand and predict the dynamic processes that occur during catalysis that change the structural and chemical nature of these particles, including the roles of changes in their electronic structures, chemical bond breaking, and chemical bond formation.[12,14−19]

Density functional theory (DFT)[20−24] is currently the method of choice[25−27] to theoretically explore the catalytic properties of small Pt-NPs and their supported complexes on titania surfaces. However, its high computational cost makes

Received: June 17, 2023
Published: August 30, 2023

ACS Publications © 2023 American Chemical Society

the dynamic calculations inaccessible for Pt-NPs with experimental size distributions and often requires the adaption of small nanoclusters to represent Pt-NPs.[28] This drawback can impose severe limitations on the studies of numerous dynamic processes that may occur during catalysis at high temperatures, such as particle diffusion, nucleation, Ostwald ripening/NP sintering, particle-phase transformations, surface reconstructions, etc. Dynamics simulations based on DFT have thus far been limited to a few short trajectories of single-atom surface diffusions at a fixed, high temperature of 927 °C,[29] and we are not aware of any reported quantum chemical free energy profiles. Thus, in order to capture more realistic chemical reaction mechanisms, the effects of Pt-NPs size, or changes to catalytic properties with temperature, it is necessary to employ a computationally more accessible method for systems with larger sizes.

To overcome the limitation of DFT, the density functional tight binding (DFTB) method[30−34] was developed for the computation of systems containing thousands of atoms with reasonable accuracy in geometry and energy comparable to DFT. The DFTB approximation to DFT is a viable candidate for more realistic investigations of dynamics and chemical reaction mechanisms. DFTB-based molecular dynamics (MD) simulations retain the electronic structure properties of the catalyst while allowing the dynamics to be explored and thus constitute an ideal method for predicting complex dynamic processes in heterogeneous catalysts, such as surface reconstruction or NP sintering at the tens of nanometers scale and at time scales longer than those used with DFT-based MD, also called *ab initio* MD.[35] However, the application of DFTB/MD for studying Pt-NPs in the vacuum or Pt-NPs on a titania support has been precluded due to the lack of corresponding parameters. Although DFTB parameters have been reported in the literature for pure Pt systems, they either severely overestimate or underestimate even the pure Pt−Pt interactions.[36−38] Furthermore, prior to the current work, no DFTB parameters are available for the Pt-X (X = Ti, O) interactions.

In this work, we built on our previously reported preliminary second-order DFTB electronic parameters for Pt[37] and developed four new sets of electronic and repulsive parameters. We further developed matching Pt-X (X = Pt, Ti, O) repulsive potentials in second-order DFTB formalism, leveraging a previous parametrization of titania.[39] The optimized DFTB parameters were validated by comparing the following reference properties, from DFT: geometries, energetic properties, and electronic structures. The test set for validation includes Pt_n (n = 2 to 116) clusters, ≈ 20,000 conformations of Pt_n (n = 10, 11, 12, 13) clusters, bulk Pt (SC, BCC, HCP, and FCC), and the chemisorption of Pt_n (n = 1 to 8) cluster on the TiO_2 rutile (110) and anatase (101) surfaces. The overall best-performing parameter set, based on our benchmark, was employed to simulate the diffusion of Pt_1 atom and the growth of Pt_6 from Pt_5 and Pt_1 on rutile (110) surface using the steered molecular dynamics (SMD) method.[40−42] The effects of temperature on the corresponding free energy profiles or potential of mean force (PMF) and the dynamics of Pt particles on the titania surface were also investigated. The newly developed DFTB parameters, previously described in the PhD thesis of one of the authors,[43] open a physics-based pathway for future reactive MD simulations of Pt-NP processes occurring at high temperatures during catalysis with the first principles of charge distribution and predictive DFT accuracy. The low computational cost of DFTB further allows the generation of exhaustive databases for machine learning potentials which are becoming increasingly popular[44] but currently lack the capability of predicting reliably charge transfer processes and catalytic reactivity.[45]

METHODOLOGY AND COMPUTATIONAL DETAILS

Overview of DFTB2. The DFTB method is an approximation to DFT based on the tight binding model, a two-center approximation, and empirical fitted pairwise potentials. In DFTB, the Coulombic interactions are explicitly considered using a Taylor expansion of the DFT energy $E[\rho]$ around a reference electron density.[30,31,46] For a given molecular or solid-state system, its electron density can be written as a sum over atomic reference and initial electron densities ρ_0 and the electron density fluctuation $\delta\rho$. By employing the Taylor expansion, the DFT energy can be expressed as

$$E[\rho] = E^0[\rho_0] + E^1[\rho_0, \delta\rho] + E^2[\rho_0, (\delta\rho)^2] + E^3[\rho_0, (\delta\rho)^3] + \ldots \quad (1)$$

where $\rho = \rho_0 + \delta\rho$. In the framework of DFTB, the expansion of DFT energy can be truncated at each energy term (E^1, E^2, or E^3) to formulate the corresponding energy for the first-order DFTB1,[30,31] second-order DFTB2,[32] and third-order DFTB3,[33,34] respectively.[47]

Detailed derivations and comprehensive reviews of the DFTB methods can be found elsewhere.[32,47−49] In this work, we solely utilize the DFTB2 method, which is also referred to as self-consistent-charge-DFTB, or (SCC)-DFTB,[32] since we aim to maintain compatibility with the corresponding, well-tested tiorg parameter set.[39] The DFTB2 total energy is defined as

$$E = \sum_i n_i \langle \Psi_i | \hat{H}[\rho_0] | \Psi_i \rangle + \frac{1}{2} \sum_{AB} \gamma_{AB} \Delta q_A \Delta q_B + \sum_{A>B} E_{AB}^{\mathrm{rep}} \quad (2)$$

where $\hat{H}[\rho_0]$ is the initial electronic Hamiltonian, $|\Psi_i\rangle$ are the occupied valence molecular orbitals (MOs), n_i are the occupation numbers, Δq_A is the Mulliken point charge[50] on atom A, $\gamma_{AB}\Delta q_A \Delta q_B$ represents the interaction energy between the two point charges,[32] and E_{AB}^{rep} is the repulsive potential between two atoms A and B. The MO $|\Psi\rangle$ can be expanded as a linear combination of optimized pseudoatomic orbitals (AOs) $|\phi_\mu\rangle$, which form the basis set in which the electronic Hamiltonian is expressed.

To obtain a suitable pseudoatomic basis set and initial atomic electron density for the chemical environment of an atom in the DFTB framework, an external confinement term was introduced to the Kohn−Sham equation of the free atom

$$\left[-\frac{1}{2}\nabla^2 + v^{\mathrm{eff}}[\rho^{\mathrm{atom}}] + \left(\frac{|\mathbf{r}|}{r_0} \right)^2 \right] \phi_\mu(\mathbf{r}) = \epsilon_\mu \phi_\mu(\mathbf{r}) \quad (3)$$

where r_0 is the empirical confinement radius parameter and ϕ_μ is the atom-centered pseudoatomic Slater-type orbitals. By solving eq 3, one can obtain various atomic orbitals and electron densities depending on confining radii r_0. Because the atomic orbital and electron density can be optimized separately, there are two types of confinement radii: one for the wave function, r^{wf}, and one for density, r^{dens} corresponding

https://doi.org/10.1021/acs.jctc.3c00661
J. Chem. Theory Comput. 2023, 19, 6471−6483

to the confined atomic orbitals (basis set) and the atomic reference electron densities, respectively. The orbital confinement has a greater effect on molecular geometries, whereas the density confinement exerts a stronger influence on the bond energies.

In the framework of the two-center approximation and the pseudoatomic basis set, the initial Hamiltonian $\hat{H}_0[\rho_0]$ is defined as

$$H^0_{\mu\nu} = \langle\phi_\mu|\hat{H}[\rho_0]|\phi_\nu\rangle \approx \begin{cases} \epsilon^{\text{free atom}}_\mu & \mu = \nu \\ \langle\phi_\mu|\hat{T} + V^{AB}|\phi_\nu\rangle & \mu \in A, \nu \in B, \mu \neq \nu \\ 0 & \text{otherwise} \end{cases} \quad (4)$$

where $V^{AB} = V[\rho^A_0 + \rho^B_0]$ in the density superposition approach or $V^{AB} = V[\rho^A_0] + V[\rho^B_0]$ in the potential superposition approach. The repulsive potential between two atoms E^{rep}_{AB} is formulated as a two-center term that depends only on the chemical element type of atoms A and B and their interatomic distance r_{AB}.[48] Practically, the repulsive potential can be defined as a combination of exponential and spline functions. The total repulsive energy is fitted to minimize the difference between DFTB electronic energies and chosen reference energies for a training set of molecular systems.[51−53] The reference energies are usually computed by high-level methods such as wave function theory (WFT) or DFT methods.

Parametrization. For the DFTB parametrization, two groups of parameters need to be determined: (1) the electronic parameters (which are composed of the confinement radii r^{wf} for the AOs basis set, the confinement radii r^{dens} for the atomic densities, and the atomic orbital energies) and (2) the pairwise repulsive potentials. While the occupied atomic orbital energies are computed directly with an atomic DFT code, the unoccupied atomic orbital energies and pairwise repulsive potentials are optimized in order to reproduce certain desired properties, for instance, electronic structures, energies, and geometries.

Pt−Pt Interactions. Given the similar atom sizes of Pt and Au, we adopted the confinement radii for the electron density r^{dens} and atomic wave functions r^{wf} of occupied atomic orbitals of Au from the "auorg" parameter set[54] for the electronic parameters of Pt. On the other hand, the atomic orbital energy and confinement radius r^{wf} of the virtual orbital 6p were systematically explored. We found that by shifting the 6p virtual orbital energy upward by 0.0345 au from the DFT-computed value or by employing a larger confinement radius r^{wf} for the virtual orbital, one can reduce the notorious overbinding of metal−metal interactions. The shift of virtual orbital energies for improving binding energies has been reported previously for gold clusters[55] and the 3d orbital for phosphorus.[56] The combination of the two options for the Pt virtual orbital energy ϵ_{6p} and the two options for the confinement radius r^{wf}_{6p} results in four sets of Pt electronic parameter sets, named pt^α, pt^β, pt^κ, and pt^γ, which are listed in Table 1.

The Pt−Pt repulsive potential was optimized for each set of electronic parameters using the genetic algorithm (GA) optimization tool we developed[53] and employed for other DFTB parameters following a similar automatic parametrization protocol.[53,56] The repulsive potentials were optimized on the basis of DFTB electronic energies to fit atomization energies, equilibrium bond distance, forces, and reaction energies for the training set listed in Tables S1, S2, and S4 in the Supporting Information. The GA was used to minimize a scoring function F^{score} defined as the fitness of the parameter sets with respect to DFTB values and reference data according to the formula

$$F^{\text{score}} = \frac{1}{N_{\text{eq}}}\left[\sum_i (w^{\text{at.}}_i \Delta E^{\text{at.}}_i)^2 + \sum_i (w^{\text{rxn}}_i \Delta E^{\text{rxn}}_i)^2 + \sum_i \sum_{j\in 3N_i} (w^{\text{force}}_i \Delta F^{\text{force}}_{i,j})^2\right] \quad (5)$$

where $\Delta E^{\text{at.}} = E^{\text{at.}}_{\text{eDFTB}} - E^{\text{at.}}_{\text{ref}}$ is the deviation in atomization energies; $\Delta E^{\text{rxn}} = E^{\text{rxn}}_{\text{eDFTB}} - E^{\text{rxn}}_{\text{ref}}$ is the deviation in reaction energies; $\Delta F^{\text{force}} = F^{\text{force}}_{\text{eDFTB}} - F^{\text{force}}_{\text{ref}}$ is the deviation in forces; $w^{\text{at.}}_i$, w^{rxn}_i, and w^{force}_i are the weight factors of the ith atomization energy, reaction energy, and the force of the ith structure, respectively; N_{eq} is the number of fitting data points; N_i is the number of atoms in the ith compound; and eDFTB stands for DFTB energy without the repulsive potential term. We employed a cutoff radius of 3.5 Å and six spline knots for the repulsive potential term with one allowable extremum and a continuity requirement up to the second derivative. For the GA optimization, population sizes of 1000 and 3000 generations were employed with two-point crossover and random mutation rates of 0.9 and 0.2, respectively.

Pt−Ti and Pt−O Interactions. As mentioned in the Results and Discussion section, the pt^α parameter set has the overall weakest performance for the Pt bulk system and thus was dropped in the parametrization for Pt−Ti and Pt−O interactions. The DFTB confinement radii for Ti and O, as well as their Ti−Ti, Ti−O, and O−O repulsive potentials were taken from the "tiorg" parameter set[39] for compatibility purposes. Combined with three new Pt parameter sets (pt^β, pt^κ, and pt^γ), three corresponding pt^β-tiorg, pt^κ-tiorg, and pt^γ-tiorg sets were created. We employed a similar fitting strategy for the Pt−Ti and Pt−O repulsive potentials as for the fitting of the Pt−Pt repulsive potential. The training set is listed in Tables S3, S5, and S6 in the Supporting Information. In addition, we applied three additional constraints to the Pt−Ti repulsive potential and empirically shifted the reference reaction energies of two reactions in Table S6 by −11 kcal/mol to improve the adsorption of Pt atoms (Pt_1) on the rutile (110) surface. We employed a cutoff radius of 3.7 and 3.4 Å for the Pt−Ti and Pt−O potentials, respectively. The same six spline knots, one allowable extremum, and a continuity requirement up to the second derivative constraints were also used. For the GA optimization, population sizes of 2000 and 3000 generations were employed with two-point crossover and random mutation rates of 0.9 and 0.2, respectively. The Pt−Ti and Pt−O potentials were optimized simultaneously.

Table 1. Atomic Virtual Orbital Energy and Compression Radii of Pt in au for Different Optimized Parameter Sets

	pt^α	pt^β	pt^κ	pt^γ
ϵ_{6p}	−0.0305	0.0040	−0.0305	0.0040
r^{wf}_{6p}	4.51	4.51	6.50	6.50
r^{wf}_{6s}	6.50	6.50	6.50	6.50
r^{wf}_{5d}	6.50	6.50	6.50	6.50
r^{dens}	9.41	9.41	9.41	9.41

https://doi.org/10.1021/acs.jctc.3c00661
J. Chem. Theory Comput. 2023, 19, 6471−6483

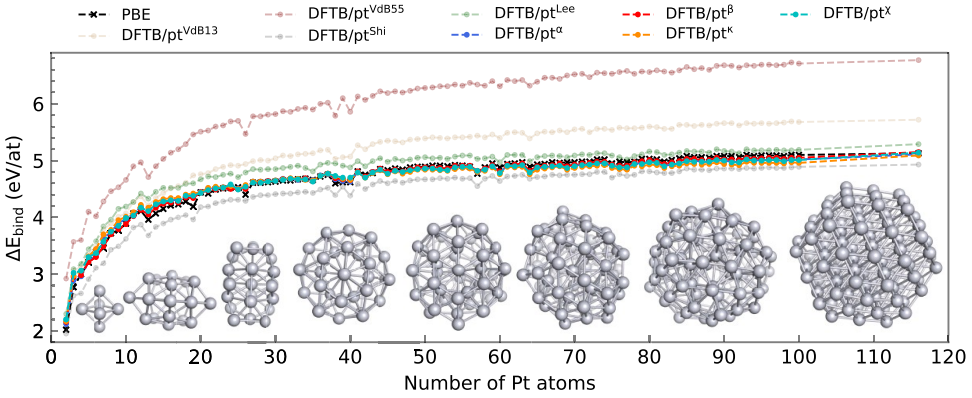

Figure 1. DFTB normalized binding energies computed with different parameter sets in comparison with the PBE normalized binding energies for Pt_2 to Pt_{116} clusters. The new parameter sets from this study (DFTB/pt^{α}, DFTB/pt^{β}, DFTB/pt^{κ}, and DFTB/pt^{χ}) reproduced energy data that closely match the PBE binding energies.

Computational Details. In this work, all DFTB calculations are spin-unpolarized and were carried out using the DFTB+ program.[57] The Perdew−Burke−Ernzerhof (PBE)[23] density functional was chosen as the reference method. For the DFT calculations, the projector augmented wave (PAW) approach[58] was used with the kinetic energy cutoff set at 450 eV and carried out using the Vienna ab initio simulation package (VASP) program in conjunction with the provided "PAW_PBE" pseudopotentials.[59,60] The convergence criteria were set to 10^{-6} eV for achieving self-consistent field energies and 0.005 eV/Å for the maximum force in the case of geometry optimizations.

Steered MD (SMD)[40] for free energy simulations via direct DFTB MD simulation was conducted using a spring force attached to the moving atom with a moving speed v = 0.01 Å/ps, a spring force constant k = 300 kcal/mol/Å^2, and a time step interval Δt = 2 fs. The Berendsen thermostat[61] was used because the system size is relatively small for other approaches. Simulated temperatures were T = 400, 600, and 800 K. Sampling was based on over a hundred trajectory replicas for each system based on Jarzynski equality[41,62−64] to compute the change in the free energy or potential of mean force (PMF). The free energy profile between two equilibrium states can be calculated from the work done on a system during a nonequilibrium process, based on the Jarzynski equality, as $\Delta F = -\frac{1}{\beta}\ln(\langle e^{-\beta W}\rangle)$, where ΔF represents the free energy difference, $\beta = \frac{1}{k_B T}$, k_B is the Boltzmann constant, T is the temperature, W denotes the work, and the angled brackets denote an ensemble average. The main challenge in applying the Jarzynski equality lies in the necessity for a substantial number of sampling data points. This requirement arises due to the dominance of small work values, which occur infrequently in the exponential average $\langle e^{-\beta W}\rangle$. To alleviate the demand for extensive sampling, we employ the second-order cumulant expansion of the Jarzynski equality developed by Park et al.[41,64] to calculate the free energy difference as $\Delta F = \langle W\rangle - \frac{\beta}{2}(\langle W^2\rangle - \langle W\rangle^2)$.

RESULTS AND DISCUSSION

As mentioned, there have been several prior DFTB parametrizations reported for pure platinum clusters and nanoparticles,[36,38] including our own preliminary work.[37] In this work, we present a comprehensive benchmark of our improved and previous parameters for platinum clusters and nanoparticles and vacuum before describing the parametrization strategy and benchmarks for Pt-NP simulations on rutile and anatase surfaces based on the existing DFTB tiorg parameters.[39] We demonstrate that DFTB/MD can be employed reliably for Pt atomic diffusion on TiO_2 surfaces and present free energy profiles for a model process of Ostwald ripening at various temperatures where a single Pt atom is incorporated into a larger Pt cluster on the rutile (110) surface.

Performance for Pure Pt Clusters, Nanoparticles, and Bulk Metal. To validate our new Pt parametrization against DFT, we compared DFTB normalized cluster binding energies, optimized geometries, and band structures to corresponding reference values computed by the PBE DFT functional for a series of Pt clusters, nanoparticles, and Pt bulk metal. The performance of our four parameter sets pt^{α}, pt^{β}, pt^{κ}, and pt^{χ} was also compared to the Pt parameters pt^{Shi} previously developed by Shi et al.,[36] pt^{Lee} reported by Lee et al.,[37] and the parameter sets pt^{VdB13} and pt^{VdB55} reported by Van den Bossche.[38]

Pt_2 to Pt_{116} Clusters. Figure 1 shows the DFTB performance in predicting binding energy for pure Pt clusters ranging from Pt_2 to Pt_{116} with structures optimized by DFT. The root-mean-square error (RMSE), mean unsigned error (MUE), mean signed error (MSE), and maximum absolute error (Max) of DFTB normalized binding energies referenced to their corresponding DFT-computed values for the test are listed in Table 2. While every parameter set in question can mimic the increase in normalized binding energy with the size of Pt clusters using DFTB, their accuracy varies drastically. DFTB/pt^{VdB13} and DFTB/pt^{VdB55} severely overestimate binding energies, particularly for large clusters, with MSE values of 0.47 and 1.32 eV/at., respectively. The large overestimation of binding energies in these parameters can be attributed to their parametrization, which focused only on relative isomer energies for fixed Pt_{13} and Pt_{55} cluster sizes, respectively. DFTB/pt^{Lee} also shows significant overbinding with an MSE of 0.18 eV/at., while DFTB/pt^{Shi} shows significant underbinding with an MSE of −0.22 eV/at. It should be noted that the latter parametrization aimed not solely at describing pure Pt nanoparticles but focused on binary clusters containing ruthenium and platinum. Our four new parameter sets generally outperform the existing parameter sets with an MSE ≈ 0.01 eV/at. and RMSE less than 0.1 eV/at. Among the

https://doi.org/10.1021/acs.jctc.3c00661
J. Chem. Theory Comput. 2023, 19, 6471−6483

Table 2. Root-Mean-Square Error (RMSE), Mean Unsigned Error (MUE), Mean Signed Error (MSE), and Maximum Absolute Error (Max) of DFTB Normalized Binding Energies Compared to PBE Normalized Binding Energies, Root-Mean-Square (RMS), Mean, and Maximum of Root-Mean-Square Deviation (RMSD) over Atomic Positions of DFTB Geometries Compared to PBE-Optimized Geometries for Pt_2 to Pt_{116} Clusters

	energy (eV/at.)				RMSD (Å)		
names	RMSE	MUE	MSE	Max	RMS	mean	Max
pt^{VdB13}	0.48	0.47	0.47	0.67	0.44	0.37	1.09
pt^{VdB55}	1.35	1.32	1.32	1.64	0.39	0.31	1.09
pt^{Shi}	0.23	0.22	−0.22	0.34	0.37	0.34	1.01
pt^{Lee}	0.20	0.18	0.18	0.41	0.15	0.14	0.30
pt^{α}	0.07	0.06	−0.01	0.19	0.18	0.16	0.36
pt^{β}	0.05	0.04	−0.01	0.18	0.17	0.16	0.36
pt^{κ}	0.10	0.09	−0.02	0.24	0.18	0.17	0.36
pt^{γ}	0.08	0.06	−0.01	0.25	0.18	0.16	0.43

four new parameter sets, pt^{β} shows the best performance with an RMSE of 0.05 eV/at.

To assess the accuracy of DFTB in predicting the structure of Pt clusters, DFTB-optimized geometries were compared to the ones mentioned above that were optimized using PBE DFT. The root-mean-square (RMS), mean, and maximum root-mean-square deviation (RMSD) over atomic positions of the test set are given in Table 2. Similar to the performance of predicting binding energies, pt^{VdB13} and pt^{VdB55} show significantly large deviations with the mean RMSD approximating 0.44 and 0.39 Å, respectively. pt^{Shi} shows a similar level of accuracy, with a large mean of RMSD of 0.34 Å. Regarding the geometry, pt^{Lee} and our new four parameter sets outperform the other parameters with a mean RMSD of less than 0.17 Å. pt^{Lee} is slightly better than the new parameter sets with a mean RMSD of 0.14 Å. Among the four new parameter sets, pt^{β} shows the best performance, with the smallest RMS of RMSD being 0.17 Å, compared to the RMS of RMSD equaling 0.18 Å in the case of pt^{α}, pt^{κ}, and pt^{γ}.

Large Set of Pt_{10}, Pt_{11}, Pt_{12}, and Pt_{13} Isomers. To further assess the accuracy of our new parameters with DFTB, their performance was evaluated for a large set of 5000 Pt_{10} isomers, 5000 Pt_{11} isomers, 5000 Pt_{12} isomers, and 4950 Pt_{13} isomers. The test set was originally reported by Fung et al.[65] and was used to test DFTB in the work of Lee et al. These geometries were taken from the work by Fung et al., and single-point energy calculations were carried out using DFTB with selected parameters. For higher accuracy, the DFT single-point energies were recomputed by using the PBE functional with a high energy cutoff of 450 eV. Figure 2 compares the DFTB-computed normalized binding energies with pt^{Shi}, pt^{Lee}, pt^{α}, and pt^{β} parameters to the DFT-computed normalized binding energies. The same comparison of DFTB energies with pt^{VdB13}, pt^{VdB55}, pt^{κ}, and pt^{γ} is shown in Figure S1 in the Supporting Information. In terms of absolute binding energies, the new parameters outperform existing parameters, similar to the "Pt_2 to Pt_{116}" test set. Significant overbinding was observed for pt^{VdB55} and pt^{Lee}, while underbinding was observed for pt^{Shi}. It is interesting to note that pt^{VdB13} shows reasonably small overbinding for Pt clusters in this range. This is likely because the parameter was originally optimized for Pt_{13} clusters. Regarding relative binding energies, pt^{VdB13} and pt^{VdB55} outperform all other parameters with an R^2 higher than 0.88, especially in the case of pt^{VdB13} with an R^2 higher than 0.95. This is expected as these parameters were optimized to predict not binding energies but the relative energy of isomers. pt^{Shi} shows the weakest correlation with R^2 ranging from 0.45 to 0.63, whereas the four new parameter sets and pt^{Lee} show a reasonably high correlation with R^2 varying from 0.74 to 0.91.

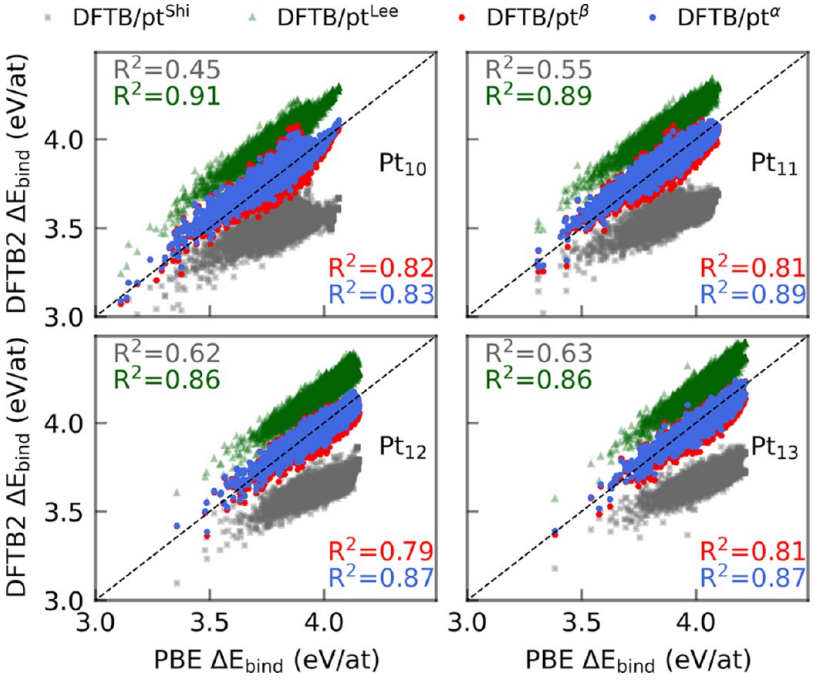

Figure 2. DFTB normalized binding energies ΔE_{bind} compared to PBE normalized binding energies ΔE_{bind} for ≈20,000 conformations of Pt_{10}, Pt_{11}, Pt_{12}, and Pt_{13} clusters. The new parameter sets from this study produced the data shown in red and blue and have significantly better parity than earlier published parameter sets.

https://doi.org/10.1021/acs.jctc.3c00661
J. Chem. Theory Comput. 2023, 19, 6471−6483

Since these roughly 20,000 structures were only partially optimized by Fung et al., they are, in fact, not suitable to validate DFTB for predicting geometries. Thus, we selected 70 isomers of Pt_{10}, 80 isomers of Pt_{11}, 90 isomers of Pt_{12}, and 100 isomers of Pt_{13} to formulate a new test set of 340 isomers of Pt_{10} to Pt_{13}. These clusters were fully reoptimized by using PBE with a higher energy cutoff of 450 eV. Table 3 shows the accuracy of DFTB with all parameters with regard to binding energy and geometry. Overall, the accuracy among all DFTB parameters is similar to that observed in the above-mentioned cases for the "Pt_2 to Pt_{116}" test set. Nevertheless, in terms of geometry, all four new parameter sets and pt^{Lee} show a slightly larger average of RMSD values compared to the previous test set. This can be attributed to the fact that the test set includes many high-energy isomers with elongated Pt−Pt bond lengths, which were purposefully added to describe processes such as Ostwald ripening but are generally more difficult to describe within the DFTB approach since it utilizes a preoptimized minimal basis set of pseudoatomic orbitals.

Table 3. Root-Mean-Square Error (RMSE), Mean Unsigned Error (MUE), Mean Signed Error (MSE), and Maximum Absolute Error (Max) of DFTB Normalized Binding Energies Compared to PBE Normalized Binding Energies, Root-Mean-Square (RMS), Mean, and Maximum of Root-Mean-Square Deviation (RMSD) over Atomic Positions of DFTB Geometries Compared to PBE-Optimized Geometries for 340 Isomers of Pt_{10} to Pt_{13} Clusters

	energy (eV/at.)				RMSD (Å)		
names	RMSE	MUE	MSE	Max	RMS	mean	Max
pt^{VdB13}	0.27	0.27	0.27	0.46	0.41	0.33	1.31
pt^{VdB55}	0.96	0.96	0.96	1.82	0.37	0.31	1.09
pt^{Shi}	0.20	0.19	−0.19	0.34	0.38	0.35	1.10
pt^{Lee}	0.25	0.25	0.25	0.41	0.22	0.18	0.71
pt^{α}	0.07	0.06	0.05	0.17	0.25	0.20	0.95
pt^{β}	0.08	0.06	0.05	0.22	0.26	0.21	0.94
pt^{κ}	0.07	0.07	0.06	0.24	0.23	0.19	0.97
pt^{χ}	0.09	0.07	0.06	0.23	0.26	0.22	0.95

Bulk Systems. Even though the main purpose of our parametrization is the description of supported Pt-NPs, we also include here the evaluation of our new Pt−Pt DFTB parameters for various properties of the platinum bulk metal in different crystal structures using PBE DFT reference data. Important quantities of interest for such a comparison include cohesive energies, lattice constants, and band structures of the bulk systems, assuming simple cubic (SC), body-centered cubic (BCC), hexagonal closest packed (HCP), and face-centered cubic (FCC) unit cells. The computed cohesive energies and lattice constants are listed in Table 4. Overall, PBE-computed lattice constants are reproduced well in all of our parametrizations, where the largest deviation observed is below 0.15 Å. On the other hand, their predicted cohesive energies are somewhat too low and vary more strongly. Nevertheless, among the four new parameters, all except pt^{α} are able to predict the order of cohesive energies increasing from SC to FCC unit cells (SC < BCC < HCP < FCC). For pt^{β}, pt^{κ}, and pt^{χ}, a significantly large underestimation of 0.5−0.7 eV in cohesive energy was observed in the case of SC and BCC unit cells. Smaller deviations of 0.1−0.2 eV were observed for the HCP and FCC unit cells. We note that in our experience cohesive energies predicted by the DFTB method are more accurate for denser and lower-energy unit cells due to the usage of a minimum basis set. Accordingly, our results highlight the limitations of tight binding approaches for higher energy systems.

Figure 3 compares DFTB/pt^{β}-computed band structures to those from the PBE for SC, BCC, HCP, and FCC unit cells. The same comparison of DFTB with pt^{α}, pt^{κ}, and pt^{χ} is shown in Figures S2−S8 in the Supporting Information. Overall, DFTB with our new parameters closely mimics PBE-computed band structures for all unit cells in the range of −5 to 5 eV, consistent with strategies outlined earlier.[52,66] Larger deviations were observed in the ranges of −10 to −5 eV and 5 to 10 eV.

Performance for Pt Clusters on Titania Support. As mentioned in the Parametrization section, only three parameter sets pt^{β}, pt^{κ}, and pt^{χ} were integrated with the "tiorg" parameter set. To evaluate the accuracy of DFTB with the newly created pt^{β}-tiorg, pt^{κ}-tiorg, and pt^{χ}-tiorg sets, we

Table 4. Cohesive Energies ΔE_{coh} and Lattice Constants Computed by DFTB with Different Parameters in Comparison to the Reference Values from PBE for Pt Simple Cubic (SC), Body-Centered Cubic (BCC), Hexagonal Closest Packed (HCP), and Face-Centered Cubic (FCC) Unit Cells

		DFTB							
	PBE	pt^{VdB13}	pt^{VdB55}	pt^{Shi}	pt^{Lee}	pt^{α}	pt^{β}	pt^{κ}	pt^{χ}
				SC					
a (Å)	2.63	2.58	2.56	2.82	2.73	2.73	2.72	2.73	2.72
ΔE_{coh} (eV/at.)	5.42	6.17	7.38	5.32	5.07	5.13	5.16	4.91	4.98
				BCC					
a (Å)	3.17	3.15	3.14	3.35	3.06	3.20	3.15	3.14	3.08
ΔE_{coh} (eV/at.)	5.78	6.72	8.08	5.49	5.52	5.10	5.21	4.96	5.13
				HCP					
a (Å)	2.77	2.75	2.73	2.92	2.81	2.80	2.78	2.79	2.77
b (Å)	2.77	2.73	2.73	2.92	2.81	2.80	2.78	2.79	2.77
c (Å)	4.78	4.78	4.73	4.81	4.82	4.70	4.68	4.67	4.65
ΔE_{coh} (eV/at.)	5.82	6.79	8.23	5.56	5.82	5.59	5.72	5.52	5.67
				FCC					
a (Å)	3.98	3.93	3.92	4.14	4.05	3.99	3.97	3.97	3.96
ΔE_{coh} (eV/at.)	5.87	6.69	8.29	5.63	5.87	5.66	5.79	5.59	5.74

https://doi.org/10.1021/acs.jctc.3c00661
J. Chem. Theory Comput. 2023, 19, 6471−6483

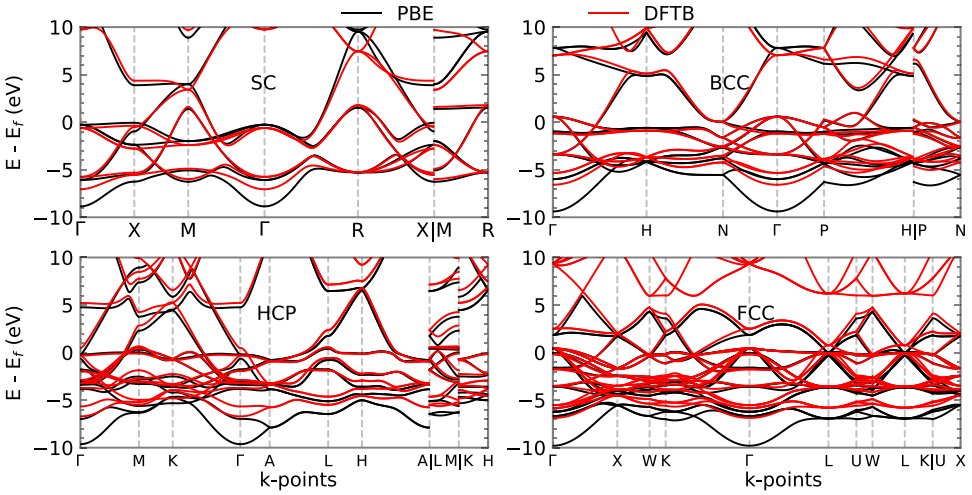

Figure 3. Band structures computed by DFTB/pt$^{\beta}$ in comparison to those from PBE for Pt simple cubic (SC), body-centered cubic (BCC), hexagonal closest packed (HCP), and face-centered cubic (FCC) unit cells.

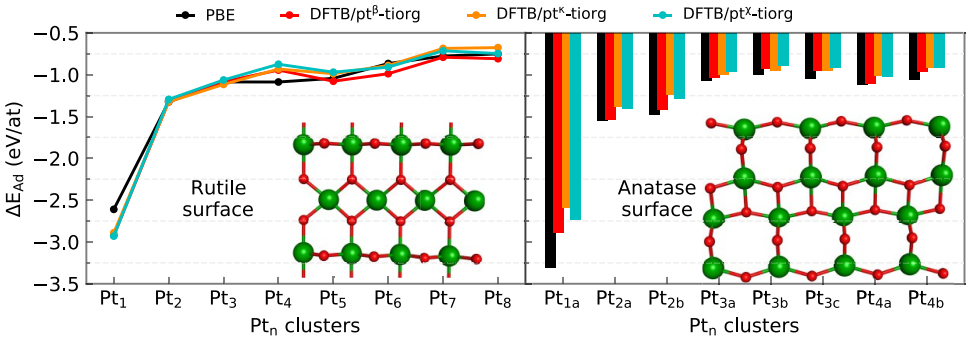

Figure 4. Normalized adsorption energies computed by DFTB with three different parameter sets in comparison to the corresponding values computed by PBE for Pt_1 to Pt_8 clusters on the TiO_2 rutile (110) surface and Pt_1 to Pt_4 clusters on the TiO_2 anatase (101) surface.

compared their binding energies, optimized and geometries computed by DFTB to their corresponding reference values computed by the PBE functional for a series of Pt_1 to Pt_8 clusters on the TiO_2 rutile (110) surface and Pt_1 to Pt_4 clusters on the TiO_2 anatase (101) surface. Additionally, the energy landscape of Pt atom adsorption on the TiO_2 rutile (110) surface was also used to assess the new parameters.

Pt_1 to Pt_8 Clusters on the TiO_2 Rutile (110) Surface and Pt_1 to Pt_4 Clusters on the TiO_2 Anatase (101) Surface. Figure 4 shows the performance of DFTB for the pt$^{\beta}$-tiorg, pt$^{\kappa}$-tiorg, and pt$^{\chi}$-tiorg parameter sets in predicting adsorption energies for Pt clusters on the titania support. The RMSE, MUE, MSE, and Max of DFTB normalized binding energies referenced to their corresponding DFT-computed values for this evaluation are given in Table 5. Overall, DFTB can reasonably well reproduce the trends of PBE-computed adsorption energies varying with the size of Pt_n clusters. While the level of fidelity is high for all sets, around the same level of accuracy for the rutile (110) surface with RMSE varying from 0.12 to 0.14 eV/at., pt$^{\beta}$-tiorg is superior when it comes to the case of the anatase (101) surface with an RMSE of 0.16 compared to an RMSE of 0.24 and 0.28 eV/at. of pt-tiorg$^{\kappa}$ and pt-tiorg$^{\chi}$, respectively.

The RMS, mean, and maximum of RMSDs between DFTB-optimized and PBE-optimized geometries for Pt clusters on the two surfaces are listed in Table 5. Overall, all three parameter sets show excellent accuracy in terms of the geometry, especially in the case of the anatase surface, with all RMS of RMSDs being smaller than 0.13 Å. In the case of the rutile surface, the RMS of RMSDs of 0.16 Å for pt$^{\beta}$-tiorg is slightly better than the other two, where values are 0.18 and 0.19 Å for pt$^{\chi}$-tiorg and pt$^{\kappa}$-tiorg, respectively. In order to visually

Table 5. Root-Mean-Square Error (RMSE), Mean Unsigned Error (MUE), Mean Signed Error (MSE), and Maximum Absolute Error (Max) of DFTB Normalized Binding Energies Compared to PBE Normalized Binding Energies, Root-Mean-Square (RMS), Mean, and Maximum of Root-Mean-Square Deviation (RMSD) over Atomic Positions of DFTB Geometries Compared to PBE-Optimized Geometries for Pt_1 to Pt_8 Clusters on the TiO_2 Rutile (110) Surface and Pt_1 to Pt_4 Clusters on the TiO_2 Anatase (101) Surface[a]

	energy (eV/at.)				RMSD (Å)		
names	RMSE	MUE	MSE	Max	RMS	mean	Max
			Rutile				
pt$^{\beta}$-tiorg	0.13	0.08	−0.05	0.31	0.16	0.15	0.22
pt$^{\kappa}$-tiorg	0.12	0.09	0.00	0.28	0.19	0.18	0.27
pt$^{\chi}$-tiorg	0.14	0.09	0.00	0.32	0.18	0.17	0.27
			Anatase				
pt$^{\beta}$-tiorg	0.16	0.10	0.10	0.42	0.12	0.10	0.27
pt$^{\kappa}$-tiorg	0.28	0.20	0.20	0.72	0.13	0.10	0.28
pt$^{\chi}$-tiorg	0.24	0.19	0.19	0.58	0.12	0.10	0.27

[a]The RMSD over atomic positions was calculated over the Pt atoms and their bonded Ti and O atoms; cutoffs of 2.8 and 2.5 Å were used to determine the bonding of Pt−Ti and Pt−O, respectively.

https://doi.org/10.1021/acs.jctc.3c00661
J. Chem. Theory Comput. 2023, 19, 6471−6483

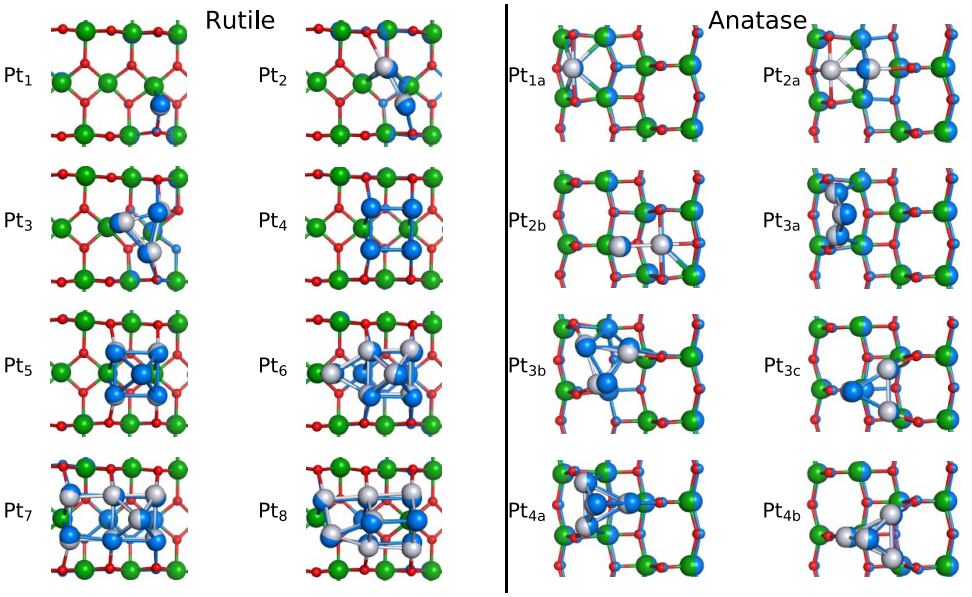

Figure 5. Overlap of PBE-optimized structures (Pt in gray, Ti in green, and O in red) and DFTB/pt$^{\beta}$-tiorg optimized structures (in sky blue) for Pt_1 to Pt_8 clusters on the TiO_2 rutile (110) surface and Pt_1 to Pt_4 clusters on the TiO_2 anatase (101) surface.

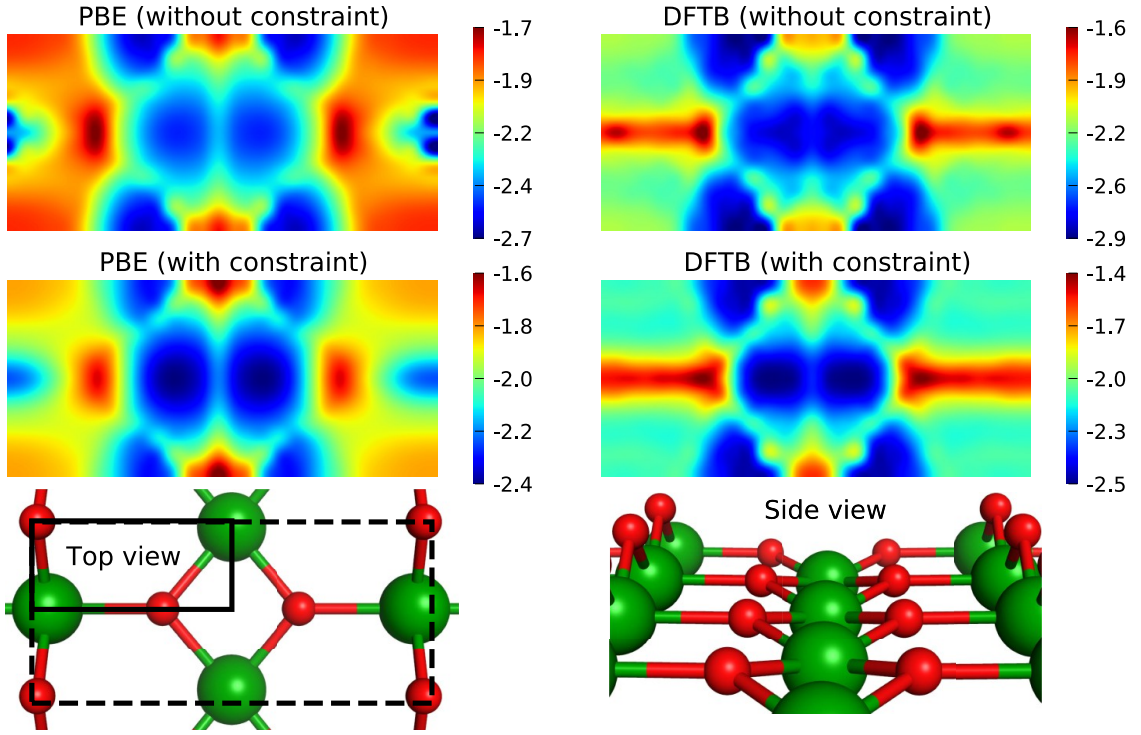

Figure 6. Energy landscape in eV of Pt atom adsorption on the TiO_2 rutile (110) surface obtained by PBE and DFTB/pt$^{\beta}$-tiorg methods. The reference energy is defined as the sum of the energies of the single Pt atom and the isolated TiO_2 rutile (110) surface; "without constraint" refers to the geometry optimization with the top two layers of TiO_2 surface fully optimized and "with constraint" refers to the geometry optimization with only a few selected Ti and O atoms nearby the Pt single atom optimized.

illustrate the differences between PBE-optimized and DFTB-optimized geometries, the overlayed atom positions of Pt clusters optimized by PBE and DFTB/pt$^{\beta}$-tiorg are shown in Figure 5. Similar comparisons for structures optimized by DFTB/pt$^{\kappa}$-tiorg and DFTB/pt$^{\chi}$-tiorg are shown in Figures S9 and S10 in the Supporting Information. The overlaid structures were determined by a minimization procedure, which includes centering and rotation to minimize the RMSD over all Pt atoms and the Ti and O atoms directly bonded to them. These structures highlight the excellent performance of DFTB in describing Pt cluster geometries on rutile and anatase surfaces.

Energy Landscape of Single Pt Atom Adsorption on the TiO_2 Rutile (110) Surface. To evaluate the transferability of the new DFTB parameters, we further explored the energy landscape of a single Pt atom adsorption on the TiO_2 rutile (110) surface and compared it with their corresponding PBE-computed energy landscape. The computed DFTB/pt$^{\beta}$-tiorg and PBE energy landscapes are shown in Figure 6. Similar

https://doi.org/10.1021/acs.jctc.3c00661
J. Chem. Theory Comput. 2023, 19, 6471−6483

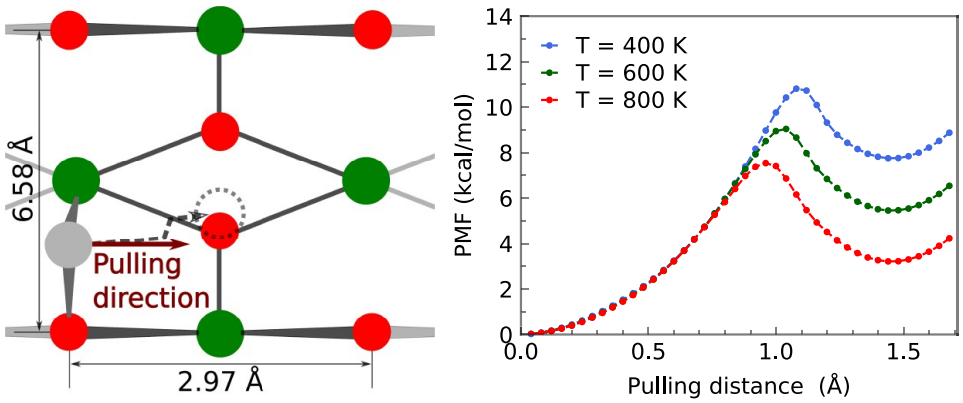

Figure 7. Potential of mean force (PMF) of single Pt atom transport on the TiO_2 rutile (110) surface at three different temperatures computed by the steered molecular dynamics (SMD) method with a pulling speed of 0.02 Å/ns.

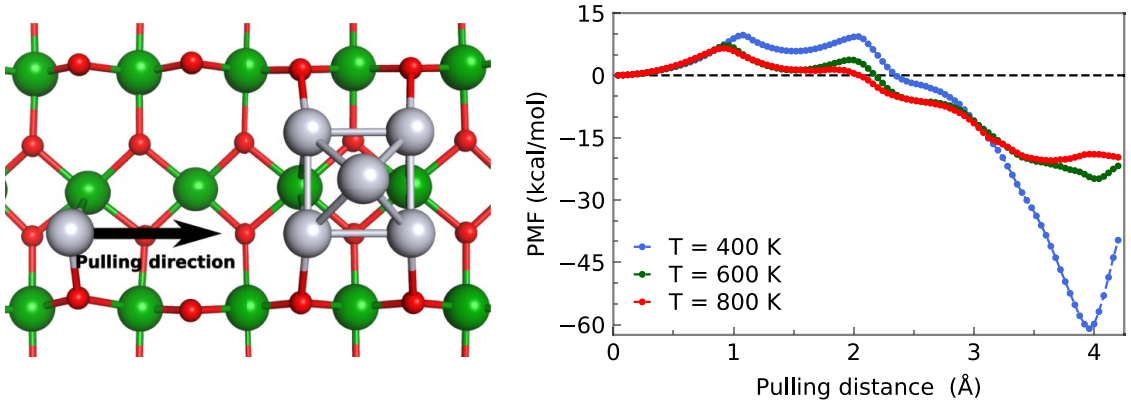

Figure 8. Potential of mean force (PMF) of growth of Pt_6 from Pt_5 and a nearby single Pt atom on the TiO_2 rutile (110) surface at three different temperatures computed by the steered molecular dynamics (SMD) method.

comparisons for energy landscapes computed by DFTB/pt$^{\kappa}$-tiorg, and DFTB/pt$^{\chi}$-tiorg are shown in Figures S11 and S12, respectively, in the Supporting Information. As discussed in previous work for the parametrization of Au−P interactions,[56] this test is particularly useful for evaluating the transferability of the new parameters, as the varying number of Ti and O atoms coordinating with the Pt atom on the surface simulates a change in the chemical coordination environment. DFTB/pt$^{\beta}$-tiorg is able to qualitatively reproduce the relative PBE energy landscape in the strong bonding "valley" on the rutile surface. However, a significant deviation is observed in the high-energy region outside this valley. Even though the significant deviation in the high-energy region implies a limit of the transferability of these parameters, it is important to note that DFTB/pt$^{\beta}$-tiorg can qualitatively mimic the shape of the PBE energy landscape between these high-energy regions with and without constraint. This suggests that the parameters can describe changes in the support surface, which is particularly important in dynamic free energy simulations of surface diffusion, which constitutes one of the goals of this work.

Diffusion of a Pt Atom on the TiO_2 Rutile (110) Surface. In order to demonstrate the applicability of our new DFTB parameters for Pt on a TiO_2 support, we employed our "best" set (DFTB/pt$^{\beta}$-tiorg) to investigate the diffusion of a Pt atom on the TiO_2 rutile (110) surface as a function of temperature relevant for catalytic processes. The free energy barrier of the diffusion as a function of temperature was estimated using the steered molecular dynamics (SMD) method[40−42] and the Jarzynski equality. The simulation was carried out by pulling a single Pt atom along the "valley" of the rutile (110) surface. The potential of mean force (PMF) was computed from the pulling work of over 100 SMD trajectories using Jarzynski equality. The SMD simulation is illustrated in Figure 7. The same figure shows the temperature dependence of the surface diffusion barrier's free energy. When the temperature increases from 400 to 800 K, the free energy barrier reduces from 11 kcal/mol to only 7 kcal/mol, which is a typical entropic effect on atom diffusion on surfaces.[67] An internal linear free energy relationship (LFER) as a function of temperature is apparent in Figure 7 between the PMF change to the barrier height ($\Delta PMF^{\ddagger}$) and the PMF change of the elementary reaction step in moving from the first adsorption site to the second (ΔPMF_{rxn}). Over the simulated temperature range, this elementary reaction step has an internal LFER of $\Delta PMF^{\ddagger} = 0.7228\ \Delta PMF_{rxn} + 5.174$ (kcal/mol). The value of 0.7228 for the slope indicates that the transition state is a late-stage transition state and more chemically similar to the "product" state (right-hand state) than to the "reactant" state (left-hand state) of Figure 7. This example demonstrates that DFTB/MD simulations are in the position to reveal insights into elementary step transition states from the temperature dependence of the PMF. These results agree with experimental data showing that the sintering process of a single Pt atom or small Pt clusters occurs much faster at increased temperatures.[67]

https://doi.org/10.1021/acs.jctc.3c00661
J. Chem. Theory Comput. 2023, 19, 6471−6483

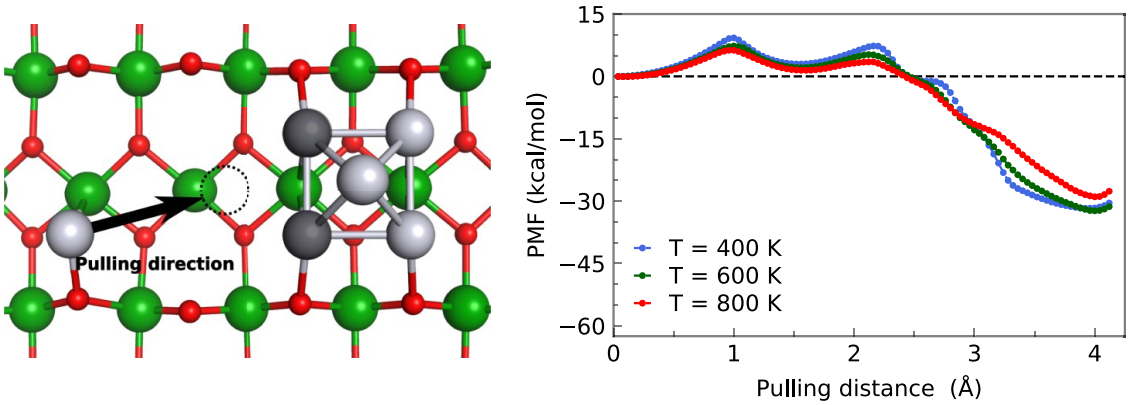

Figure 9. Potential of mean force (PMF) of growth of Pt_6 from Pt_5 and a nearby single Pt atom on the TiO_2 rutile (110) surface at three different temperatures computed by the steered molecular dynamics (SMD) method. An additional restraint was applied to the Pt_5 cluster to reduce its dynamic along the reaction coordinate, with a pulling speed v = 0.02 Å/ns.

Growth of Pt_6 from Pt_5 and Pt_1 on the TiO_2 Rutile (110) Surface. To further understand Pt-NP growth events and the effect of the temperature, we employ DFTB/pt^{β}-tiorg to investigate the growth of Pt_6 from Pt_5 and Pt_1 on the TiO_2 rutile (110) surface. Similar to the study of Pt diffusion, the SMD method was used to accelerate the event. A single Pt atom was pulled toward the Pt_5 cluster, as illustrated in Figure 8. Again, the potential of mean force (PMF) was computed from the pulling work of over 100 SMD trajectories using Jarzynski's equality. While the effects of temperature on the amplitude of the first barrier are similar to the case of single Pt atom diffusion on the surface, the second barrier changed drastically with the temperature. The second barrier was reduced from 11 kcal/mol at 400 K to ≈0 kcal/mol at 800 K. By analyzing the SMD trajectories, we found that the lowering second energy barrier is due to the dynamics of the preexisting Pt_5 cluster as it deforms its structure and "reaches out" toward the approaching Pt single atom at the position of the second energy barrier. This distortion of the Pt_5 cluster induces the early formation of the Pt_5+Pt_1 complex, stabilizing the transition state and affording a lower Pt_6 cluster geometry. Since the final Pt_6 cluster geometry can vary significantly due to the distortion of Pt_5 and the early formation of the Pt_5+Pt_1 complex. It is necessary to be careful to associate the resulting PMF only with pulling the single Pt atom after crossing the second energy barrier, and the observed barrier does not reflect the free energy of formation for a "static" attachment of Pt_1 to Pt_5 to grow into Pt_6.

To estimate the effect of temperature on the free energy of formation for Pt_6 from Pt_5 and Pt_1 more consistently, without considering Pt_5 cluster distortions, we employed an additional geometry restraint on two Pt atoms of the preexisting Pt_5 cluster in order to restrict the movement of the cluster toward the single Pt atom. The simulation is illustrated in Figure 9. With the extra restraint on the Pt_5 cluster, the drastic changes found previously in the second energy barrier at high temperatures were eliminated, confirming that the decrease in energy originated from distortion of the Pt_5 cluster. A total free energy decrease of ≈30 kcal/mol associated with the Pt_6 growth process was observed. The increase in temperature affects the total free energy of formation for Pt_6 from Pt_5 and Pt_1 as well. However, the change of only a few kcal/mol is small compared to the total formation energy of ≈30 kcal/mol. In conclusion, increasing temperatures significantly reduces the energy barrier of Pt atom transport on the TiO_2 surface and the transition state (TS) of its deposition while having a minimal effect on the formation free energy. Therefore, increasing temperature enhances the growth event, e.g., during Ostwald ripening, in agreement with experimental observations.[12]

CONCLUSIONS

We present a computationally affordable methodology for the first-principles-based quantum chemical simulation of free energy changes in Pt-NP supported on titania at finite temperatures. This methodology is based on the density functional tight binding (DFTB) method for the direct calculation of energies and gradients in steered molecular dynamics (SMD) or similar biased MD simulations. Four DFTB parameter sets were developed and rigorously benchmarked against first-principles DFT with the PBE functional for the energetics and geometries of platinum particles in the vacuum, bulk Pt, and Pt clusters on TiO_2 support. The four parameter sets are distinguished by exploring two different choices for the virtual Pt 6p atomic orbital energy and its wave function compression radius, as this orbital participates in metal−metal bonds, and its energy and size must be finely tuned to compensate for the deficiencies of the minimum basis set employed in tight binding schemes.[56] One of the four parameter sets (pt^{α}) is found inferior to the other three in terms of energies and geometries of bulk Pt and was not extensively documented here. The other three are similar in accuracy and were analyzed and found to accurately predict the geometries, energetic properties, and electronic structures of various Pt_n clusters and the chemisorption of Pt_n (n = 1 to 8) clusters on the TiO_2 rutile (110) and anatase (101) surfaces as well as to be sufficiently accurate for the qualitative description of potential energy surfaces of platinum single-atom adsorbed on the titania rutile surface. The pt^{β} parameter was found to have a slightly better overall performance for the energetic and structural description of platinum clusters on titania; therefore, we employed it in subsequent DFTB/SMD simulations of Pt atom surface diffusion and Pt cluster growth as a result of atom attachment.

The DFTB/SMD simulations were carried out in canonical MD simulations at constant temperatures of 400, 600, and 800 K, using over 100 trajectories for each temperature and system. We found that increasing the temperature has a considerable effect on the apparent free energy barrier for atom diffusion and decreases with increased temperature, as discussed

https://doi.org/10.1021/acs.jctc.3c00661
J. Chem. Theory Comput. 2023, 19, 6471−6483

previously by Tully et al.[67] for adatom diffusion phenomena. We then simulated the growth of Pt_6 from Pt_5 via the atom attachment of Pt_1 on the rutile (110) surface. In this case, increasing the temperature had a minimal effect on the formation free energy of the product Pt_6 cluster. A considerable contribution to such dynamic processes can occur from dynamic changes in the Pt-NPs themselves. Such phenomena are considered important to understand temperature-dependent growth/sintering Pt-NP dynamics on the titania support at the atomic level.

To the best of our knowledge, the reported simulations are the first quantum chemical simulations of the free energy profiles for metal nanoparticles on titania support on the atomic scale. With the new parameters and the combined DFTB/SMD methodology, it becomes possible to simulate the dynamics of platinum nanoparticles on titania surfaces, providing insights into diffusion, sintering events, and temperature effects. This is the necessary first step toward DFTB-based studies of surface dynamic evolution processes occurring at Pt clusters on TiO_2 support interfaces and paving the way for future improvements in platinum catalysts.

■ ASSOCIATED CONTENT

Supporting Information

The Supporting Information is available free of charge at https://pubs.acs.org/doi/10.1021/acs.jctc.3c00661.

Expressions for evaluation metrics, information for the training sets, optimized geometries used in the training sets, and additional benchmark results (PDF)

Geomfiles (ZIP)

■ AUTHOR INFORMATION

Corresponding Authors

Van-Quan Vuong − *Bredesen Center for Interdisciplinary Research and Graduate Education, University of Tennessee, Knoxville, Tennessee 37996, United States;* Present Address: Department of Chemistry, Boston University, Boston, Massachusetts 02215, United States; orcid.org/0000-0001-8580-8532; Email: qvuong@alum.utk.edu

Stephan Irle − *Computational Sciences & Engineering Division, Oak Ridge National Laboratory, Oak Ridge, Tennessee 37831, United States; Bredesen Center for Interdisciplinary Research and Graduate Education, University of Tennessee, Knoxville, Tennessee 37996, United States;* orcid.org/0000-0003-4995-4991; Email: irles@ornl.gov

Authors

Ka Hung Lee − *Bredesen Center for Interdisciplinary Research and Graduate Education, University of Tennessee, Knoxville, Tennessee 37996, United States;* orcid.org/0000-0003-1429-7872

Aditya A. Savara − *Chemical Sciences Division, Oak Ridge National Laboratory, Oak Ridge, Tennessee 37831, United States;* orcid.org/0000-0002-1937-2571

Victor Fung − *Center for Nanophase Materials Sciences, Oak Ridge National Laboratory, Oak Ridge, Tennessee 37831, United States;* Present Address: School of Computational Science and Engineering, Georgia Institute of Technology, Atlanta, Georgia 30332, United States; orcid.org/0000-0002-3347-6983

Complete contact information is available at: https://pubs.acs.org/10.1021/acs.jctc.3c00661

Notes

The authors declare no competing financial interest.

Notice of Copyright: This manuscript was authored by UT-Battelle, LLC under Contract DE-AC05−00OR22725 with the U.S. Department of Energy. The United States Government retains and the publisher, by accepting the article for publication, acknowledges that the United States Government retains a nonexclusive, paid-up, irrevocable, worldwide license to publish or reproduce the published form of this manuscript, or allow others to do so, for United States Government purposes. The Department of Energy will provide public access to these results of federally sponsored research in accordance with the DOE Public Access Plan (http://energy.gov/downloads/doe-public-access-plan).

■ ACKNOWLEDGMENTS

The authors thank Gang Seob Jung (ORNL) and De-en Jiang (Vanderbilt University) for their helpful suggestions and discussions. The foundation of this manuscript is based on the contents of chapter 4 of Van-Quan Vuong's PhD dissertation, titled "Development of Density-Functional Tight-Binding Methods for Chemical Energy Science," which was submitted to the University of Tennessee in 2021.[43] V.Q.V and K.H.L. were supported by an Energy Science and Engineering Fellowship from the Bredesen Center for Interdisciplinary Research and Graduate Education at the University of Tennessee, Knoxville. This work was sponsored by the U.S. Department of Energy, Office of Science, Office of Basic Energy Sciences, Chemical Sciences, Geosciences, and Biosciences Division, Catalysis Science Program. This research used resources of the National Energy Research Scientific Computing Center (NERSC), a U.S. Department of Energy Office of Science User Facility operated under Contract No. DE-AC02-05CH11231, as well as cloud resources of the Compute and Data Environment for Science (CADES) at Oak Ridge National Laboratory, which is supported by the Office of Science of the U.S. Department of Energy under Contract No. DE-AC05-00OR22725.

■ REFERENCES

(1) Liu, Q.; Zhang, Z. Platinum Single-Atom Catalysts: A Comparative Review towards Effective Characterization. *Catal. Sci. Technol.* **2019**, *9*, 4821−4834.

(2) Xu, J.; Liu, X.; Zhou, Z.; Deng, L.; Liu, L.; Xu, M. Platinum Nanoparticles with Low Content and High Dispersion over Exfoliated Layered Double Hydroxide for Photocatalytic CO_2 Reduction. *Energy Fuels* **2021**, *35*, 10820−10831.

(3) Ehelebe, K.; Knöppel, J.; Bierling, M.; Mayerhöfer, B.; Böhm, T.; Kulyk, N.; Thiele, S.; Mayrhofer, K. J. J.; Cherevko, S. Platinum Dissolution in Realistic Fuel Cell Catalyst Layers. *Angew. Chem., Int. Ed.* **2021**, *60*, 8882−8888.

(4) Huang, L.; Zaman, S.; Tian, X.; Wang, Z.; Fang, W.; Xia, B. Y. Advanced Platinum-Based Oxygen Reduction Electrocatalysts for Fuel Cells. *Acc. Chem. Res.* **2021**, *54*, 311−322.

(5) Yang, A.-c.; Zhu, H.; Li, Y.; Cargnello, M. Support Acidity Improves Pt Activity in Propane Combustion in the Presence of Steam by Reducing Water Coverage on the Active Sites. *ACS Catal.* **2021**, *11*, 6672−6683.

(6) Campbell, C. T. Metal Films and Particles on Oxide Surfaces: Structural, Electronic and Chemisorptive Properties. *J. Chem. Soc., Faraday Trans.* **1996**, *92*, 1435.

(7) Campbell, C. T. Ultrathin Metal Films and Particles on Oxide Surfaces: Structural, Electronic and Chemisorptive Properties. *Surf. Sci. Rep.* **1997**, *27*, 1−111.
(8) Jeantelot, G.; Qureshi, M.; Harb, M.; Ould-Chikh, S.; Anjum, D. H.; Abou-Hamad, E.; Aguilar-Tapia, A.; Hazemann, J.-L.; Takanabe, K.; Basset, J.-M. TiO_2 -Supported Pt Single Atoms by Surface Organometallic Chemistry for Photocatalytic Hydrogen Evolution. *Phys. Chem. Chem. Phys.* **2019**, *21*, 24429−24440.
(9) Hejazi, S.; Mohajernia, S.; Osuagwu, B.; Zoppellaro, G.; Andryskova, P.; Tomanec, O.; Kment, S.; Zbořil, R.; Schmuki, P. On the Controlled Loading of Single Platinum Atoms as a Co-Catalyst on TiO_2 Anatase for Optimized Photocatalytic H_2 Generation. *Adv. Mater.* **2020**, *32*, 1908505.
(10) Hao, H.; Jin, B.; Liu, W.; Wu, X.; Yin, F.; Liu, S. Robust Pt@ TiOx/TiO_2 Catalysts for Hydrocarbon Combustion: Effects of Pt-TiOx Interaction and Sulfates. *ACS Catal.* **2020**, *10*, 13543−13548.
(11) Chen, L.; Unocic, R. R.; Hoffman, A. S.; Hong, J.; Braga, A. H.; Bao, Z.; Bare, S. R.; Szanyi, J. Unlocking the Catalytic Potential of TiO_2 -Supported Pt Single Atoms for the Reverse Water−Gas Shift Reaction by Altering Their Chemical Environment. *JACS Au* **2021**, *1*, 977−986.
(12) Hansen, T. W.; DeLaRiva, A. T.; Challa, S. R.; Datye, A. K. Sintering of Catalytic Nanoparticles: Particle Migration or Ostwald Ripening? *Acc. Chem. Res.* **2013**, *46*, 1720−1730.
(13) Almeida, L. D.; Wang, H.; Junge, K.; Cui, X.; Beller, M. Recent Advances in Catalytic Hydrosilylations: Developments beyond Traditional Platinum Catalysts. *Angew. Chem., Int. Ed.* **2021**, *60*, 550−565.
(14) Pan, Y.; Hwang, S. Y.; Shen, X.; Yang, J.; Zeng, J.; Wu, M.; Peng, Z. Computation-Guided Development of Platinum Alloy Catalyst for Carbon Monoxide Preferential Oxidation. *ACS Catal.* **2018**, *8*, 5777−5786.
(15) He, Y.; Liu, J.-C.; Luo, L.; Wang, Y.-G.; Zhu, J.; Du, Y.; Li, J.; Mao, S. X.; Wang, C. Size-Dependent Dynamic Structures of Supported Gold Nanoparticles in CO Oxidation Reaction Condition. *Proc. Natl. Acad. Sci. U.S.A.* **2018**, *115*, 7700−7705.
(16) Weerawardene, K. D. M.; Häkkinen, H.; Aikens, C. M. Connections Between Theory and Experiment for Gold and Silver Nanoclusters. *Annu. Rev. Phys. Chem.* **2018**, *69*, 205−229.
(17) Parrish, K. A.; King, M.; Ligare, M. R.; Johnson, G. E.; Hernández, H. Role of Sterics in Phosphine-Ligated Gold Clusters. *Phys. Chem. Chem. Phys.* **2019**, *21*, 1689−1699.
(18) Lim, J. S.; Vandermause, J.; van Spronsen, M. A.; Musaelian, A.; Xie, Y.; Sun, L.; O'Connor, C. R.; Egle, T.; Molinari, N.; Florian, J.; Duanmu, K.; Madix, R. J.; Sautet, P.; Friend, C. M.; Kozinsky, B. Evolution of Metastable Structures at Bimetallic Surfaces from Microscopy and Machine-Learning Molecular Dynamics. *J. Am. Chem. Soc.* **2020**, *142*, 15907−15916.
(19) Sun, G.; Fuller, J. T.; Alexandrova, A. N.; Sautet, P. Global Activity Search Uncovers Reaction Induced Concomitant Catalyst Restructuring for Alkane Dissociation on Model Pt Catalysts. *ACS Catal.* **2021**, *11*, 1877−1885.
(20) Hohenberg, P.; Kohn, W. Inhomogeneous Electron Gas. *Phys. Rev.* **1964**, *136*, B864−B871.
(21) Kohn, W.; Sham, L. J. Self-Consistent Equations Including Exchange and Correlation Effects. *Phys. Rev.* **1965**, *140*, A1133−A1138.
(22) Perdew, J. P.; Chevary, J. A.; Vosko, S. H.; Jackson, K. A.; Pederson, M. R.; Singh, D. J.; Fiolhais, C. Atoms, Molecules, Solids, and Surfaces: Applications of the Generalized Gradient Approximation for Exchange and Correlation. *Phys. Rev. B* **1992**, *46*, 6671−6687.
(23) Perdew, J. P.; Burke, K.; Ernzerhof, M. Generalized Gradient Approximation Made Simple. *Phys. Rev. Lett.* **1996**, *77*, 3865−3868.
(24) Perdew, J. P.; Burke, K.; Wang, Y. Generalized Gradient Approximation for the Exchange-Correlation Hole of a Many-Electron System. *Phys. Rev. B* **1996**, *54*, 16533−16539.
(25) Nørskov, J. K.; Abild-Pedersen, F.; Studt, F.; Bligaard, T. Density Functional Theory in Surface Chemistry and Catalysis. *Proc. Natl. Acad. Sci. U.S.A.* **2011**, *108*, 937−943.
(26) Greeley, J. Theoretical Heterogeneous Catalysis: Scaling Relationships and Computational Catalyst Design. *Annu. Rev. Chem. Biomol. Eng.* **2016**, *7*, 605−635.
(27) Matera, S.; Schneider, W. F.; Heyden, A.; Savara, A. Progress in Accurate Chemical Kinetic Modeling, Simulations, and Parameter Estimation for Heterogeneous Catalysis. *ACS Catal.* **2019**, *9*, 6624−6647.
(28) Jiang, D.-e.; Overbury, S. H.; Dai, S. Structures and Energetics of Pt Clusters on TiO_2: Interplay between Metal−Metal Bonds and Metal−Oxygen Bonds. *J. Phys. Chem. C* **2012**, *116*, 21880−21885.
(29) Humphrey, N.; Bac, S.; Mallikarjun Sharada, S. Ab Initio Molecular Dynamics Reveals New Metal-Binding Sites in Atomically Dispersed Pt_1/TiO_2 Catalysts. *J. Phys. Chem. C* **2020**, *124*, 24187−24195.
(30) Porezag, D.; Frauenheim, Th.; Köhler, Th.; Seifert, G.; Kaschner, R. Construction of Tight-Binding-like Potentials on the Basis of Density-Functional Theory: Application to Carbon. *Phys. Rev. B* **1995**, *51*, 12947−12957.
(31) Seifert, G.; Porezag, D.; Frauenheim, Th. Calculations of Molecules, Clusters, and Solids with a Simplified LCAO-DFT-LDA Scheme. *Int. J. Quantum Chem.* **1996**, *58*, 185−192.
(32) Elstner, M.; Porezag, D.; Jungnickel, G.; Elsner, J.; Haugk, M.; Frauenheim, Th.; Suhai, S.; Seifert, G. Self-Consistent-Charge Density-Functional Tight-Binding Method for Simulations of Complex Materials Properties. *Phys. Rev. B* **1998**, *58*, 7260−7268.
(33) Yang, Y.; Yu, H.; York, D.; Cui, Q.; Elstner, M. Extension of the Self-Consistent-Charge Density-Functional Tight-Binding Method: Third-Order Expansion of the Density Functional Theory Total Energy and Introduction of a Modified Effective Coulomb Interaction. *J. Phys. Chem. A* **2007**, *111*, 10861−10873.
(34) Gaus, M.; Cui, Q.; Elstner, M. DFTB3: Extension of the Self-Consistent-Charge Density-Functional Tight-Binding Method (SCC-DFTB). *J. Chem. Theory Comput.* **2011**, *7*, 931−948.
(35) Marx, D.; Hutter, J. Ab Initio Molecular Dynamics: Theory and Implementation. In *Modern Methods and Algorithms of Quantum Chemistry*; John von Neumann Institute for Computing, 2000; Vol. *1*.
(36) Shi, H.; Koskinen, P.; Ramasubramaniam, A. Self-Consistent Charge Density-Functional Tight-Binding Parametrization for Pt−Ru Alloys. *J. Phys. Chem. A* **2017**, *121*, 2497−2502.
(37) Lee, K. H.; Van Vuong, Q.; Fung, V.; Jiang, D.-e.; Irle, S. Density-Functional Tight-Binding for Platinum Clusters and Bulk: Electronic vs Repulsive Parameters. *MRS Adv.* **2019**, *4*, 1821−1832.
(38) Van den Bossche, M. DFTB-Assisted Global Structure Optimization of 13- and 55-Atom Late Transition Metal Clusters. *J. Phys. Chem. A* **2019**, *123*, 3038−3045.
(39) Dolgonos, G.; Aradi, B.; Moreira, N. H.; Frauenheim, T. An Improved Self-Consistent-Charge Density-Functional Tight-Binding (SCC-DFTB) Set of Parameters for Simulation of Bulk and Molecular Systems Involving Titanium. *J. Chem. Theory Comput.* **2010**, *6*, 266−278.
(40) Isralewitz, B.; Gao, M.; Schulten, K. Steered Molecular Dynamics and Mechanical Functions of Proteins. *Curr. Opin. Struct. Biol.* **2001**, *11*, 224−230.
(41) Park, S.; Schulten, K. Calculating Potentials of Mean Force from Steered Molecular Dynamics Simulations. *J. Chem. Phys.* **2004**, *120*, 5946−5961.
(42) Chen, L. Y. Exploring the Free-Energy Landscapes of Biological Systems with Steered Molecular Dynamics. *Phys. Chem. Chem. Phys.* **2011**, *13*, 6176.
(43) Vuong, V.-Q. *Development of Density-Functional Tight-Binding Methods for Chemical Energy Science*. Ph.D. thesis, The University of Tennessee, 2021.
(44) Sumaria, V.; Nguyen, L.; Tao, F. F.; Sautet, P. Atomic-Scale Mechanism of Platinum Catalyst Restructuring under a Pressure of Reactant Gas. *J. Am. Chem. Soc.* **2023**, *145*, 392−401.

https://doi.org/10.1021/acs.jctc.3c00661
J. Chem. Theory Comput. 2023, 19, 6471−6483

(45) Schlexer Lamoureux, P.; Winther, K. T.; Garrido Torres, J. A.; Streibel, V.; Zhao, M.; Bajdich, M.; Abild-Pedersen, F.; Bligaard, T. Machine Learning for Computational Heterogeneous Catalysis. *ChemCatChem* **2019**, *11*, 3581−3601.
(46) Foulkes, W. M. C.; Haydock, R. Tight-Binding Models and Density-Functional Theory. *Phys. Rev. B* **1989**, *39*, 12520−12536.
(47) Gaus, M.; Cui, Q.; Elstner, M. Density Functional Tight Binding: Application to Organic and Biological Molecules. *WIREs Comput. Mol. Sci.* **2014**, *4*, 49−61.
(48) Elstner, M.; Seifert, G. Density Functional Tight Binding. *Philos. Trans. R. Soc., A* **2014**, *372*, 20120483.
(49) Spiegelman, F.; Tarrat, N.; Cuny, J.; Dontot, L.; Posenitskiy, E.; Martí, C.; Simon, A.; Rapacioli, M. Density-Functional Tight-Binding: Basic Concepts and Applications to Molecules and Clusters. *Adv. Phys. X* **2020**, *5*, 1710252.
(50) Mulliken, R. S. Electronic Population Analysis on LCAO−MO Molecular Wave Functions. I. *J. Chem. Phys.* **1955**, *23*, 1833−1840.
(51) Gaus, M.; Chou, C.-P.; Witek, H.; Elstner, M. Automatized Parametrization of SCC-DFTB Repulsive Potentials: Application to Hydrocarbons. *J. Phys. Chem. A* **2009**, *113*, 11866−11881.
(52) Chou, C.-P.; Nishimura, Y.; Fan, C.-C.; Mazur, G.; Irle, S.; Witek, H. A. Automatized Parameterization of DFTB Using Particle Swarm Optimization. *J. Chem. Theory Comput.* **2016**, *12*, 53−64.
(53) Vuong, V. Q.; Akkarapattiakal Kuriappan, J.; Kubillus, M.; Kranz, J. J.; Mast, T.; Niehaus, T. A.; Irle, S.; Elstner, M. Parametrization and Benchmark of Long-Range Corrected DFTB2 for Organic Molecules. *J. Chem. Theory Comput.* **2018**, *14*, 115−125.
(54) Fihey, A.; Hettich, C.; Touzeau, J.; Maurel, F.; Perrier, A.; Köhler, C.; Aradi, B.; Frauenheim, T. SCC-DFTB Parameters for Simulating Hybrid Gold-Thiolates Compounds. *J. Comput. Chem.* **2015**, *36*, 2075−2087.
(55) Oliveira, L. F. L.; Tarrat, N.; Cuny, J.; Morillo, J.; Lemoine, D.; Spiegelman, F.; Rapacioli, M. Benchmarking Density Functional Based Tight-Binding for Silver and Gold Materials: From Small Clusters to Bulk. *J. Phys. Chem. A* **2016**, *120*, 8469−8483.
(56) Vuong, V. Q.; Madridejos, J. M. L.; Aradi, B.; Sumpter, B. G.; Metha, G. F.; Irle, S. Density-Functional Tight-Binding for Phosphine-Stabilized Nanoscale Gold Clusters. *Chem. Sci.* **2020**, *11*, 13113−13128.
(57) Hourahine, B.; Aradi, B.; Blum, V.; et al. DFTB+, a Software Package for Efficient Approximate Density Functional Theory Based Atomistic Simulations. *J. Chem. Phys.* **2020**, *152*, 124101.
(58) Blöchl, P. E. Projector Augmented-Wave Method. *Phys. Rev. B* **1994**, *50*, 17953−17979.
(59) Kresse, G.; Furthmüller, J. Efficiency of Ab-Initio Total Energy Calculations for Metals and Semiconductors Using a Plane-Wave Basis Set. *Comput. Mater. Sci.* **1996**, *6*, 15−50.
(60) Kresse, G.; Furthmüller, J. Efficient Iterative Schemes for Ab Initio Total-Energy Calculations Using a Plane-Wave Basis Set. *Phys. Rev. B* **1996**, *54*, 11169−11186.
(61) Berendsen, H. J. C.; Postma, J. P. M.; van Gunsteren, W. F.; DiNola, A.; Haak, J. R. Molecular Dynamics with Coupling to an External Bath. *J. Chem. Phys.* **1984**, *81*, 3684−3690.
(62) Jarzynski, C. Equilibrium Free-Energy Differences from Nonequilibrium Measurements: A Master-Equation Approach. *Phys. Rev. E* **1997**, *56*, 5018−5035.
(63) Jarzynski, C. Nonequilibrium Equality for Free Energy Differences. *Phys. Rev. Lett.* **1997**, *78*, 2690−2693.
(64) Park, S.; Khalili-Araghi, F.; Tajkhorshid, E.; Schulten, K. Free Energy Calculation from Steered Molecular Dynamics Simulations Using Jarzynski's Equality. *J. Chem. Phys.* **2003**, *119*, 3559−3566.
(65) Fung, V.; Jiang, D.-e. Exploring Structural Diversity and Fluxionality of Pt_n (n = 10−13) Clusters from First-Principles. *J. Phys. Chem. C* **2017**, *121*, 10796−10802.
(66) Wahiduzzaman, M.; Oliveira, A. F.; Philipsen, P.; Zhechkov, L.; van Lenthe, E.; Witek, H. A.; Heine, T. DFTB Parameters for the Periodic Table: Part 1, Electronic Structure. *J. Chem. Theory Comput.* **2013**, *9*, 4006−4017.
(67) Tully, J. C.; Gilmer, G. H.; Shugard, M. Molecular Dynamics of Surface Diffusion. I. The Motion of Adatoms and Clusters. *J. Chem. Phys.* **1979**, *71*, 1630−1642.

https://doi.org/10.1021/acs.jctc.3c00661
J. Chem. Theory Comput. 2023, 19, 6471−6483